PROCEEDINGS OF SPIE

SPIEDigitalLibrary.org/conference-proceedings-of-spie

Nanometer scale imaging with table top extreme ultraviolet sources

Przemyslaw W. Wachulak, Richard L. Sandberg, Artak Isoyan, Lukasz Urbanski, Andrzej Bartnik, et al.

Przemyslaw W. Wachulak, Richard L. Sandberg, Artak Isoyan, Lukasz Urbanski, Andrzej Bartnik, Randy A. Bartels, Carmen S. Menoni, Henryk Fiedorowicz, Jorge J. Rocca, Mario C. Marconi, "Nanometer scale imaging with table top extreme ultraviolet sources," Proc. SPIE 7746, 17th Slovak-Czech-Polish Optical Conference on Wave and Quantum Aspects of Contemporary Optics, 774609 (14 December 2010); doi: 10.1117/12.880340

Event: 17th Slovak-Czech-Polish Optical Conference on Wave and Quantum Aspects of Contemporary Optics, 2010, Liptovsky Jan, Slovakia

SPIE.

Downloaded From: https://www.spiedigitallibrary.org/conference-proceedings-of-spie on 02 Aug 2019 Terms of Use: https://www.spiedigitallibrary.org/terms-of-use

Nanometer scale imaging with table top extreme ultraviolet sources

Przemyslaw W. Wachulak*[a], Richard L. Sandberg[b], Artak Isoyan[c], Lukasz Urbanski[d], Andrzej Bartnik[a], Randy A. Bartels[d], Carmen S. Menoni[d], Henryk Fiedorowicz[a], Jorge J. Rocca[d] and Mario C. Marconi[d]

[a] Institute of Optoelectronics, Military University of Technology, 00-908 Warsaw, Poland
[b] Center for Advanced Solar Photophysics, Chemistry Division, Los Alamos National Laboratory, New Mexico 87544, USA
[c] Center for Nano Technology, University of Wisconsin-Madison, Wisconsin 53706, USA
[d] NSF ERC for Extreme Ultraviolet Science & Technology and Department of Electrical and Computer Engineering, Colorado State University, Fort Collins, CO 80523 USA

ABSTRACT

Decreasing the illumination wavelength allows to improve the spatial resolution in photon-based imaging systems and enables a nanometer-scale spatial resolution. Due to a significant interest in nanometer-scale spatial resolution imaging short wavelengths from extreme ultraviolet (EUV) region are often used. A few examples of various imaging techniques, such as holography, zone plate EUV microscopy, computer generated hologram EUV reconstruction, lens-less diffraction imaging and generalized Talbot self-imaging will be presented utilizing coherent and incoherent EUV sources. Some of these EUV imaging techniques lead to the high spatial resolution, better than 50nm in a very short exposure time. The techniques, presented herein, have potential to be used in actinic mask inspection for EUV lithography, mask-less lithographic processes in the nanofabrication, in material science or biology.

Keywords: EUV holography, computer generated holograms, Talbot imaging, lens-less diffraction imaging, Fresnel zone plate microscopy, nanometer resolution, coherent EUV imaging, incoherent EUV imaging,

1. INTRODUCTION

The paper focuses on different approaches to the extreme ultraviolet imaging with the goal to show a few examples of different techniques, currently pursuit in the field of high resolution EUV imaging, capable of resolving features smaller than 100nm. The paper is organized as follows. After the introduction in this Section, Section 2 describes the EUV sources used in the imaging experiments. Majority of the experiments, presented herein, are coherent imaging techniques, such as 2-D and 3-D EUV holography – section 3, reconstruction of a computer generated hologram, fabricated by an electron beam lithography and reconstructed optically at EUV wavelength – section 3.3, high resolution imaging based on a Talbot effect – section 4, diffractive lens-less coherent imaging – section 5, requiring coherent EUV illumination. Thus for these experiments EUV source, namely a capillary discharge laser, developed at Colorado State University, was used. However, section 6 describes an example of incoherent EUV imaging performed utilizing a Fresnel optic – a zone plate. As an incoherent EUV source the laser plasma source based on a double stream gas puff target was used. This source was developed at the Military University of Technology. Finally, Section 7 contains a brief summary of each technique and the conclusions.

2. EUV SOURCES

In all coherent imaging experiments, a table top discharge pumped capillary Ne-like Ar laser, initially introduced in [1] and further developed in [2,3] was used. Figure 1a) is a photograph of the laser and the exposure chamber. The compact Ne-like Ar capillary discharge laser can be configured to produce pulses with energy ranging from 0.1 to 0.8mJ and about 1.2ns FWHM duration. It can be operated at repetition rates of several Hz, producing EUV pulses with average power in excess of 1mW with high degree of spatial and temporal coherence. The laser operates in the 46.9nm $3s^1P1$-$3p^1S0$ transition of neon-like Ar. An alumina capillary 3.2mm in diameter and 27cm in length filled with Ar is excited with a

17th Slovak-Czech-Polish Optical Conference on Wave and Quantum Aspects of Contemporary Optics, edited by Jarmila Müllerová, Dagmar Senderáková, Stanislav Jurecka, Proc. of SPIE Vol. 7746, 774609 · © 2010 SPIE · CCC code: 0277-786X/10/$18 · doi: 10.1117/12.880340

Downloaded From: https://www.spiedigitallibrary.org/conference-proceedings-of-spie on 02 Aug 2019
Terms of Use: https://www.spiedigitallibrary.org/terms-of-use

current pulse ~22kA, a 10% to 90% rise time of ~55ns and a first half-cycle duration of ~135ns. The capillary discharge laser (CDL) is based on high-gain amplification of spontaneous emission and generates a beam with high spatial and temporal coherence. The longitudinal coherence length is determined by the Doppler-broadened linewidth of the laser transition at $\Delta\lambda/\lambda=10^{-4}$, corresponding to a coherence length of 470 μm. The degree of spatial coherence increases with the length of the plasma column (capillary) and approaches full coherence for 36 cm long capillaries [4].

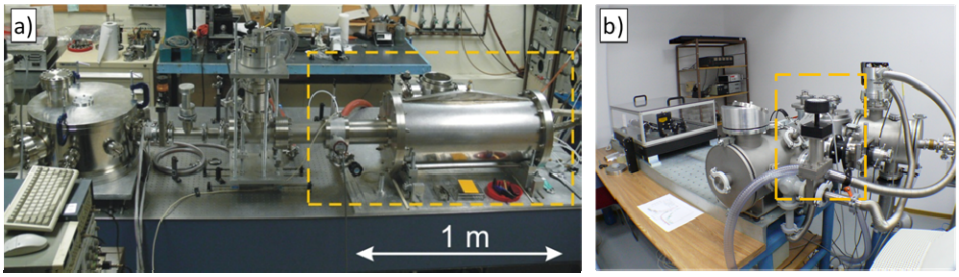


Figure 1. Compact EUV sources: capillary discharge EUV laser a) and laser plasma EUV source based on a gas puff target b).

In the extreme ultraviolet microscope using a Fresnel optic and described in Section 6, the coherence of the source can introduce additional and unwanted coherence effects, related to the properties of the laser beams [5]. Thus for this type of imaging an incoherent, compact laser plasma EUV source based on a double stream gas-puff target, presented in Figure 1b), was utilized [6]. The source was developed for EUV metrology applications under the MEDEA+ project and was studied and characterized in details elsewhere [7], however it was also optimized for EUV imaging [8]. Infrared (IR) laser pulses, λ=1064nm wavelength, 737mJ energy per pulse and 4ns time duration from a commercial Nd:YAG laser - NL 303HT (Eksma) was focused using an f=25mm focal length lens onto a double stream gas puff target. The target is produced by an electromagnetic double nozzle valve system: a round inner nozzle with a diameter of 0.4mm and ring-shaped outer nozzle with diameters of 0.7 and 1.5mm. For imaging a working gas was argon because of its narrow-band emission around 13.5nm wavelength. To achieve an optimum working gas density at certain distance away from the nozzle output a low-Z (helium) outer gas, was used. The flow of the outer gas confines the working gas towards the nozzle axis thus decreasing the density gradient of the working gas. The focused IR beam produces plasma that radiates outward in a very broad range of wavelengths, including EUV range (5-50nm), that can be used for imaging or other applications.

3. EXTREME ULTRAVIOLET HOLOGRAPHY

Holography is a well known technique, originally proposed in 1948 by Gabor, which allows recording the amplitude and phase of an electromagnetic wavefront [9]. This idea was soon extended to X-ray region by Baez [10] taking an advantage of short wavelength. However, the idea was not widely applied until the early 1960s, following the paper by Leith and Upatnieks, who proposed the off-axis holography scheme, which overcomes many of the Gabor configuration drawbacks [11]. Since then the holography was widely used in numerous applications, some of them requiring an increased spatial resolution. To improve the spatial resolution in holographic imaging, a straight forward way is to reduce the illumination wavelength [12]. This is the reason why short wavelength sources, such as synchrotrons, EUV and SXR lasers and high harmonic generation (HHG) sources are an interesting alternative for high resolution imaging.

Even though the potential for holography in the EUV spectral region was recognized very early, it was not till 1970s, when the first images of very simple objects were obtained for the first time [13,14]. The main obstacle to record and reconstruct good quality holograms in the EUV region was the lack of bright and coherent sources. Some early experiments utilized synchrotron light to image biological samples, nano structures, and magnetic domains [15, 16.] The first demonstration of a coherent table-top imaging achieved 7μm spatial resolution with a spatially-coherent HHG source [17], later improved to 0.8μm [18]. Time resolved holographic imaging was also implemented with HHG sources to study the ultrafast dynamics of surface deformation with a longitudinal resolution of less than 100nm and a lateral resolution of less than 80μm [19].

Downloaded From: https://www.spiedigitallibrary.org/conference-proceedings-of-spie on 02 Aug 2019
Terms of Use: https://www.spiedigitallibrary.org/terms-of-use

3.1 2-D, wavelength resolution holographic imaging at EUV wavelengths

The acquisition of holographic images is a process consisting of two steps: a recording and a reconstruction. During the recording step, the interference pattern between two mutually coherent beams: the reference and the object beams, is stored in a recording medium. The recording medium can be any material or device that can provide a linear mapping between the incident intensity and the medium change such as reflection, transmission or height modulation.

In our experiments a high spatial resolution photoresist was used for the recording of large numerical aperture (NA) holograms [20-22]. After developing, the holographic interference pattern was translated into a relief pattern in the surface of the photoresist and digitized using an atomic force microscope (AFM). The digitized hologram was used as an input for a code that numerically reconstructs the image using a Fresnel propagator. More details about the reconstruction algorithm can be found in [23-25].

The resolution of the holographic recording, expressed by Equation (1), is dictated by the numerical aperture $NA = n \cdot \sin(\Theta)$, where Θ is the maximum half-angle of the cone of light that can enter the imaging system, n is the index of refraction of the medium. Also, the spatial resolution depends on the resolution of the recording medium. Consequently, the highest spatial frequency that can be recorded in the recording medium sets a limit to the *NA*. To avoid this limitation the holograms were recorded in a high resolution photoresist, polymethyl methacrylate (PMMA), that has a spatial resolution of ~10nm for e-beam exposure [26,27]. The spatial resolution of the hologram is also limited by the spatial and temporal coherence of the illumination source and by the digitization process as described in more details in [12].

$$\Delta = \frac{a \cdot \lambda}{NA} \tag{1}$$

where $a \in <0.3,1>$ depending on the method used to measure the resolution and coherence of the source [28], λ is the wavelength of the illumination and *NA* is the numerical aperture of the system.

Decreasing the distance between the object and the recording medium, z_p, increases the NA and allows for storing in the photoresist's surface finer interference fringes, thus improving the spatial resolution. During the reconstruction, the AFM scan has to be large enough and with a sufficiently fine sampling to read these fringes, to be able to reconstruct the information about corresponding spatial frequency components in the final, reconstructed image. Image resolution Δ scales as $N_{total} \sim \Delta^{-4}$, as reported in [12], which imposes a practical limitation if the distance z_p is not kept small. Due to the fact that the number of points per scan line in the AFM is often limited to 1024, 2048 etc., the best option to increase the NA is to decrease the distance z_p.

The experiments, described in the next paragraph and reported in [20-22], show that increasing the NA of the recording and reconstruction opens a possibility to reach the resolution in holographic imaging comparable to the wavelength of illumination.

For hologram recording the CDL was configured to produce 0.1 mJ pulses at a repetition rate of 1 Hz. With a ratio $\lambda/\Delta\lambda \approx 10^4$, the laser has a longitudinal coherence length $l_c \approx 470$ μm. Radius of coherence - R_c, defining the spatial coherence, at the location of the experimental setup and for 28cm long capillary was estimated to be ~0.5mm. Using the Gabor's in-line geometry, where AFM tip, used as object, is directly illuminated with the laser beam, two holograms with two different NA were obtained by changing the distance z_p. Two selected object-detector distances were $z_p \approx 4$ mm (NA = 0.038) and $z_p \approx 120$ μm (NA = 0.172). The details about the recording medium and the developing procedure are described in detail in [20-22]. The exposure of ~100 EUV pulses was adjusted to achieve the linear response of the photoresist to EUV light and consequently the relief pattern height printed in its surface was equivalent to the interference intensity pattern of the hologram. Figure 2a) shows the hologram for low, NA = 0.038 recording with a total scan area ~300x300 μm^2, and a pixel size corresponding to 270 nm while Figure 2b) is the digitized hologram with the higher NA = 0.172. In this case the area scanned is 42x42 μm^2 with a pixel size equivalent to 41 nm. Developed photoresist surface was mapped with the AFM to generate digitized holograms that were reconstructed numerically by the Fresnel propagator code.

Figure 2c) and Figure 2d) are, respectively, the reconstructed images of the corresponding holograms shown in Figure 2a) and Figure 2b). The triangular profile of the AFM tip is clearly revealed. The optimum spatial resolution was assessed performing a 2-D correlation with a synthesized image – template, used as the reference image, as described in more detail in [29]. For 4mm separation the analysis indicates that the reconstructed image has a resolution equivalent to Δ=380 nm, while for 0.12mm separation the spatial resolution of the reconstruction was estimated to be Δ=164 nm. Based on the NA of the recording set up, the spatial resolution limited by the Rayleigh criterion $\Delta = (0.61\ \lambda)/NA$ gives a value Δ_R=166 nm that compares very well with the correlation analysis result.

Downloaded From: https://www.spiedigitallibrary.org/conference-proceedings-of-spie on 02 Aug 2019
Terms of Use: https://www.spiedigitallibrary.org/terms-of-use

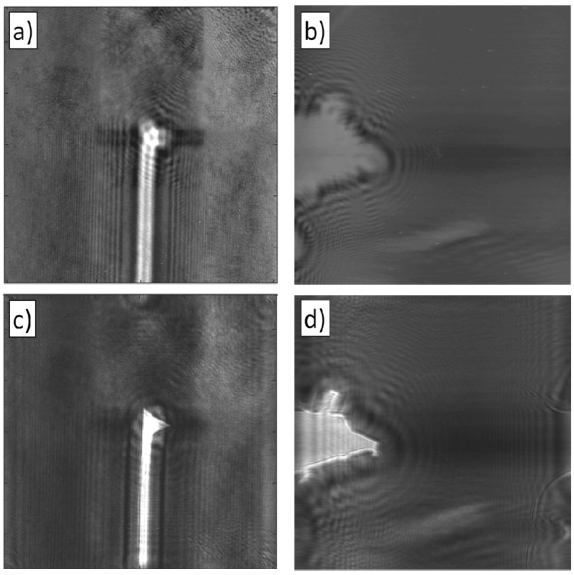


Figure 2. a,b) EUV holograms recorded at low (NA=0.038) and higher (NA=0.172) numerical apertures and corresponding reconstructions c,d) obtained using Fresnel propagator code.

Finally to further improve the spatial resolution and to reach the resolution limit imposed by the wavelength, according to Equation (1), the z_p distance was further reduced. A new object was composed of carbon nanotubes (CNT), 50-80 nm diameter and 10-20 μm in length, placed on a 100 nm thick silicon membrane acting as a support. The object is illuminated by the CDL in a Gabor's in-line configuration. The thin Si membrane has a transparency of approximately 60% at λ = 46.9 nm [30]. The CNT sample was placed approximately z_p = 2.6 μm away from a 120 nm thick PMMA layer deposited on a Si wafer. The limited area of the AFM digitization (9.9×9.9 μm^2) sets the NA to 0.88. The same procedure was used to process the hologram and reconstruct the images. Figure 3a) shows the hologram digitized with the AFM. The corresponding numerical reconstruction is shown in Figure 3b). The CNTs are clearly visible as white lines in a black background.

The spatial resolution in the reconstructed image was found applying the knife-edge test. It is based on measuring the 10-90% intensity rise in line-cuts made in a region where a "plateau" in the maximum and minimum intensities was clearly reached. The example of such line-cut is depicted in Figure 3c).

The resolution was found to be 45.8±1.9 nm, ~0.98λ, where the error is assigned by the standard deviation [22]. Additionally a global assessment of the image spatial resolution was performed, based on a correlation analysis [29] between the reconstructed hologram and a 2-D set of templates with calibrated resolution and diameter resembling the shape of the nanotubes. This method yielded a similar spatial resolution 47.5±5 nm, while allowed to determine the mean diameter of the carbon nanotubes as well: 70.6±5 nm.

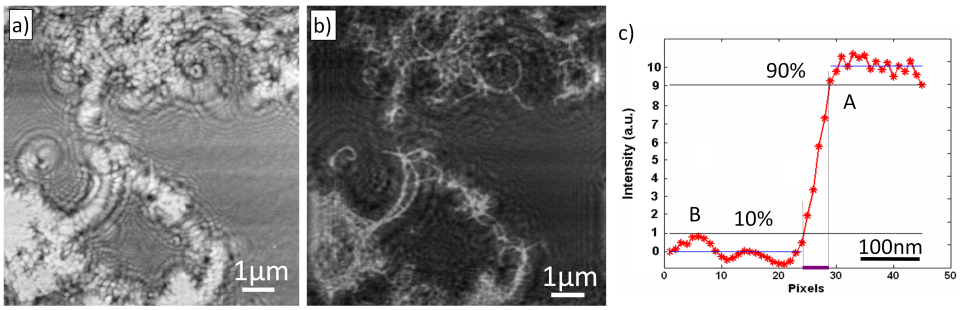


Figure 3. Hologram recorded at NA=0.88 and digitized with the AFM a), corresponding numerical reconstruction b), knife-edge resolution assessment in the reconstructed image.

Downloaded From: https://www.spiedigitallibrary.org/conference-proceedings-of-spie on 02 Aug 2019
Terms of Use: https://www.spiedigitallibrary.org/terms-of-use

3.2 3-D, holographic imaging at EUV wavelengths

The possibility of volume three dimensional imaging by the numerical sectioning obtained from a single high numerical aperture hologram, reported in [12, 21], will be discussed in this section. Three dimensional images were obtained from Gabor holograms recorded in the photoresist after exposure using the CDL. Digitized holograms were numerically reconstructed over the range of image planes by numerically sweeping the reconstruction distance, resulting in numerical optical sectioning of image depths.

The test object, used in the holographic volume imaging experiment, was fabricated by covering a semicircular hole 1.5 mm in diameter made in an 80 μm thick Mylar sheet with a 100 nm thick aluminum foil. The hole was partially covered with a second, similar Mylar sheet. The Al foil produces a variable height surface with desirable characteristics for this test; it has transmission of ~35% at λ=46.9 nm, found in [30], and suppresses the long wavelength background from the CDL. A 465 nm in diameter spherical markers [31] were randomly deposited on top of a partially transparent, tilted Al foil. These spheres are completely opaque to the 46.9 nm EUV laser radiation. To activate the PMMA exposures in the range of ~ 2×10^7 photons μm^{-2} equivalent to ~240 laser shots are required. Figure 4a) shows a small (42×42 μm^2) section of the hologram. An example of the numerical reconstruction is shown in Figure 4b).

One of the critical parameters in the reconstruction code is the z_p distance. Small changes in z_p reconstructs slightly different images. To determine the value of z_p corresponding to the optimum reconstruction for each marker, a 2-D image correlation was used and is described in details in references [20,21] and [29]. Different runs produce different reconstructed images in which the markers located at the correct z_p (boxed region in the hologram and the reconstruction) generate sharper image than those markers "out of focus". This can be observed in Figure 4c,d) where the intensity profiles obtained in a vertical profiles of one "in focus" marker (c) and one "out of focus" marker (d) are plotted. Using the correlation analysis the optimal z_p was found for each marker, completing the set of 3-D coordinates necessary to locate each marker uniquely in the 3-D space. This is the optical sectioning performed on a digitally reconstructed image. Figure 4e,f) show the surface topographies obtained from the correlation code for two different regions of the object: in the higher slope region close to the edge of the Mylard spacer e), and lower slope, at a distance approximately 200 μm away from this edge f).

The statistical dispersions of the data points relative to the best linear fit for each slope are Δz = 2.64 μm for the higher slope and Δz = 1.32 μm for the lower slope. This spread in the measured heights of the markers compares well with the expected accuracy in the z direction determined by the NA of the hologram, $\delta z = \lambda / NA^2$ [32]: the higher slope NA at z_p = 160 μm is 0.13, yielding a depth of focus δz = 2.77 μm and the lower slope region at z_p = 140 μm, NA=0.148 and δz = 2.12 μm.

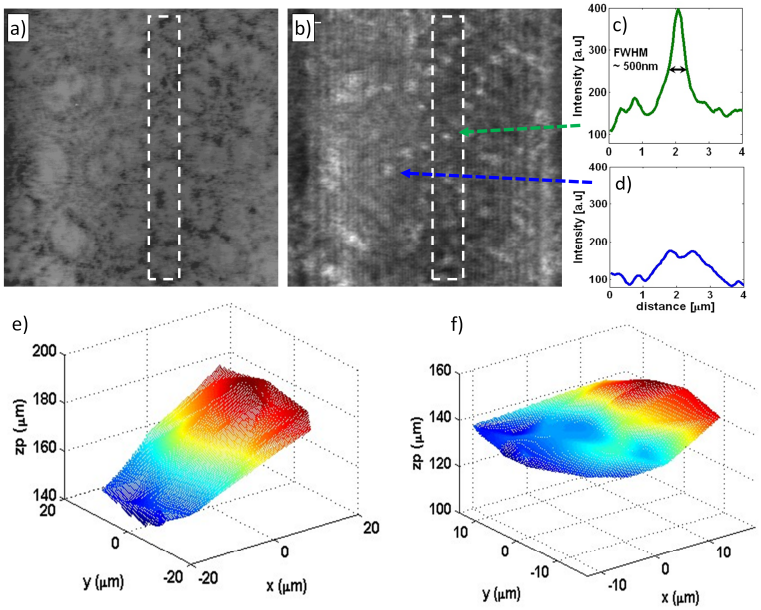


Figure 4. Small (42×42 μm^2) section of the hologram digitized with AFM a), reconstructed at the single plane (z_p=const) b), intensity profiles showing the markers "in focus" c) and "out of focus" d). Surface topographies reconstructed from the hologram for the high slope region e) and low slope region f) of the object.

Downloaded From: https://www.spiedigitallibrary.org/conference-proceedings-of-spie on 02 Aug 2019
Terms of Use: https://www.spiedigitallibrary.org/terms-of-use

3.3 EUV reconstruction of a computer generated hologram

Reconstruction of computer generated holograms (CGH) is a technique based on an optical reconstruction of a computer pre-design and fabricated hologram. It is of a particular interest to the lithographic community, because it allows to reconstruct the hologram in the surface of the photoresist at certain distance (non-contact method), particularly at the EUV wavelengths, since the EUV Lithography is one of the most promising candidates for the next generation lithographic processes capable to achieve the sub-32nm node. Moreover this technique, sometimes called holographic projection lithography, allows to generate arbitrary structures [33, 34], but it requires a coherent source for illumination, which in the EUV range of wavelengths is a severe restriction. To achieve sufficient degree of coherence strong filtering is often necessary for the coherent EUV sources, which limits the available photon flux and increases the necessary exposure. Thus the development of compact and high flux EUV sources opens a new way to use efficiently this type of coherent imaging in EUV lithography. The combination of high energy EUV lasers with the CGH reconstruction technique shows a new approach to pattern nanostructures in a versatile and efficient way.

In this section initial results of the optical reconstruction of computer generated nano-holograms at the EUV wavelength, leading to nano-structures patterned in a photoresist, are presented. The results were reported in [35]. In the experiment the CDL was used, however high requirements for the spatial coherence lead to the necessity to increase the distance between the laser and the experimental arrangement to ~2.2m. At that distance the coherence radius at the recording plane is approximately 740 μm. Due to the restrictions of the electron beam fabrication method, binary holograms were designed and generated using a half-tone optimization algorithm to improve the image quality. CGHs were fabricated on a 25 nm thick silicon nitride Si_3N_4 membrane spin-coated with 65 nm thick hydrogen silsesquioxane (HSQ) photoresist layer that acts as an absorber for the e-beam. Two SEM images of different holograms corresponding to the different arrangement line-patterns (top-left corner), presented in Figure 5a,b), were generated and later optically reconstructed.

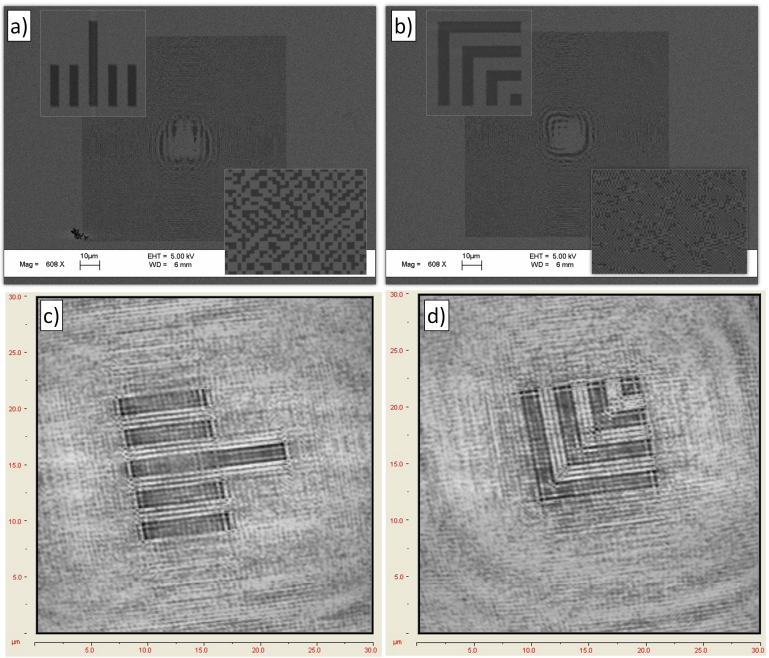


Figure 5. Different arrangement line-patterns a, b) corresponding to binary CGH c,d) respectively. The insets show the binary structure of the holograms. The scale bar is 10μm. EUV reconstruction c,d) of the CGH recorded in the PMMA photoresist for two patterns shown in a,b), respectively. Images are 30x30μm^2.

The line-width in each pattern was set to 1.54μm and each hologram size was ~103x103 μm^2. Because the size of the hologram is much less than the radius of coherence of the CDL beam, we assumed, that the hologram was illuminated by a fully spatially coherent EUV beam. The holograms were designed for a 500 μm focal plane distance (reconstruction distance) at 46.9 nm wavelength. This leads to the numerical aperture of the holograms NA=0.102. The resolution, defined by the numerical aperture, was estimated to be ~230nm and the depth of focus equal to 4.5μm. The

Downloaded From: https://www.spiedigitallibrary.org/conference-proceedings-of-spie on 02 Aug 2019
Terms of Use: https://www.spiedigitallibrary.org/terms-of-use

pixel size of the hologram is 140x140 nm^2. The insets, in low-right corner, show the binary structure of the hologram and the half-tone optimization algorithm results at high magnification. The CDL laser beam illuminates the hologram, placed at the focal distance away from the PMMA photoresist, where the reconstruction takes place. Later the PMMA photoresist is developed and scanned with the atomic force microscope. Figure 5c,d) depict the atomic force microscope scan of the reconstructed holograms recorded in the PMMA resist. The reconstructions clearly resemble the initial patterns.

4. GENERALIZED TALBOT IMAGING

The principle of generalized Talbot imaging (GTI) is based on the assumption that any two-dimensional arbitrary, periodical pattern will form self-images if illuminated by a spatially coherent beam, at the propagation distance $z=z_T$, as long as the periodicity in the two orthogonal directions is the same. Talbot distance is described by Equation (3):

$$z_T = \frac{2p^2}{\lambda} \tag{3}$$

where p is the period of the structure and λ is the illumination wavelength.

To improve the resolution, by increasing the NA of the mask containing periodically arranged pattern, the pattern, or the unit cell, is repeated multiple times in both orthogonal directions. At a certain z_T distance, after illumination by the spatially coherent beam, the reconstructed image is formed by the superposition of the diffracted orders coming from all the contributing unit cells. It is an important advantage of this technique since any defects, if present in some cells, are averaged out and contribute very little energy to the image power spectrum.

For the demonstration of GTI at EUV wavelength of 46.9nm, reported in [36], the CDL was used. Similarly, the spatial coherence of the EUV radiation was increased to reach the coherence radius of 740μm at the distance where the exposure takes place. The CDL illuminates the Talbot mask placed 219.5cm away from the laser. The size of the single Talbot mask is 600x600μm^2. The Talbot mask was fabricated on a Si_3N_4 membrane patterned using e-beam lithography in HSQ photoresist layer, 65 nm thick. The first Talbot plane was located at z_T=1 mm from the mask. Each Talbot cell, 4.84x4.84μm^2 in size, was repeated 124 times in the horizontal and vertical directions to provide an effective NA of 0.28 in order to have a point resolution λ/(2NA) equal to 84nm. The SEM images of the small section of Talbot masks are shown in Figure 6a-c). More details about the design of the mask can be found in [36].

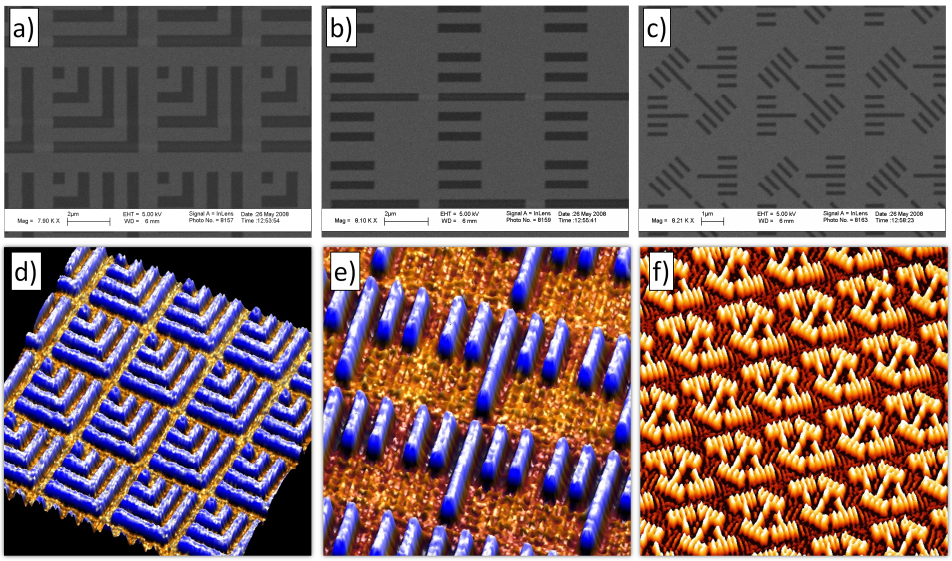


Figure 6. a,b and c) SEM images of the Talbot mask fabricated by the e-beam in the HSQ photoresist. The scale bar is 2μm. Corresponding self-images (in false colors) of the Talbot mask in the 1st Talbot plane d,e,f).

A PMMA coated sample was placed at the z_T distance of the first Talbot plane, where the self-image of the Talbot mask was formed and recorded in the photoresist. Typical patterns, shown in false colors, obtained by scanning the

Downloaded From: https://www.spiedigitallibrary.org/conference-proceedings-of-spie on 02 Aug 2019
Terms of Use: https://www.spiedigitallibrary.org/terms-of-use

PMMA surface with the AFM, are shown in Figure 6d-f) and correspond to the SEM images of the mask, depicted in Figure 6a-c). The self-images clearly resemble the masks. This clearly demonstrates the excellent imaging fidelity of this non-contact technique. The smallest features, present in the mask, Figure 6c), were 140nm wide and are clearly seen in Figure 6f). The Talbot reconstructions were recorded up to the 6th Talbot plane, with good results, which was reported in [36].

This technique opens very interesting imaging possibilities, because it does not rely on complex optical systems but rather on the fundamental principles such as diffraction and free-space propagation. However, the Talbot imaging is limited by the ability to fabricate the mask, the wavelength and degree of coherence of the source.

5. LENS LESS DIFFRACTIVE IMAGING

Currently, X-ray crystallography is the primary methodology used to determine the 3D structure of materials and macromolecules. However, many materials such as nanostructures or biological specimens are non-crystalline, thus their structures are not accessible by the X-ray crystallography. Visualizing these structures therefore requires a different approach. A very promising technique is EUV diffraction microscopy, or lens-less microscopy where the coherent diffraction pattern of a non-crystalline specimen is recorded [37]. The specimen is illuminated by a coherent light and the detailed and oversampled diffraction pattern is collected without any additional optics. Due to the phase loss a computerized phase-retrieval algorithm iteratively solves for the phase and allows to reconstruct the shape of the object. Since the first experimental demonstration in 1999, reported in [38], short wavelength diffraction microscopy has been successfully applied for imaging of nanoscale materials, structures [39] and biological cells [40], achieving spatial resolution as small as 50 nm utilizing λ=1.5nm source [41]. Furthermore, in combination with free electron laser (FEL) sources this technique has the potential for imaging of large macromolecules, without the need for crystallization in a single-shot [42, 43]. Also it eliminates the aberrations from optical elements and the need for precise sample positioning, thus allowing for near diffraction-limited resolution in EUV and SXR range of wavelengths. However, it requires very bright and fully coherent illumination.

In this section EUV diffraction microscopy using tabletop, coherent EUV source – CDL, is presented [44]. The experimental setup that fit on a 4' x 8' optical table includes both the source and the microscope. The capillary discharge laser was configured to produce EUV pulses of energy ~0.1mJ with ~4.5 mrad divergence at a repetition rate of 1 Hz. Coherent beam from the CDL laser is focused onto a sample using two Mo/Si mirrors (R~40% for an unpolarized light), flat and a 50 cm radius of curvature. Light scattered from the object is then collected using a CCD camera, Andor, 13.5x13.5μm^2 pixel size in a 2048 x 2048 array. During the acquisition a single 100 nm thick Al filter was used to block plasma emission at longer wavelengths. The sample was placed on a two-axis piezo stage, approximately 2-4 cm from the camera, to oversample the diffraction pattern and capture the highest angle diffraction speckles. Beam blocks of varying sizes were used to block out the central part of the diffraction pattern to increase the dynamic range of the recorded pattern beyond the dynamic range of the camera.

In the lens-less diffractive imaging the object must be illuminated by a coherent wavefront, must be isolated - surrounded by a substantial opaque or transparent region and the scattered light must be collected with sufficient spatial resolution to oversample the diffraction pattern, at a frequency higher than the Nyquist frequency [45]. This condition is satisfied by setting the geometry of the imaging system to sample the smallest diffraction speckle linearly by two or more CCD pixels. The linear oversampling ratio is then given by:

$$O = \frac{z\lambda}{pD} \tag{4}$$

where z is the sample to CCD distance, λ is the wavelength, D is the sample diameter, and p is the pixel size of the CCD camera [46]. The sample size is D=7 μm, the sample to CCD distance is 17 mm, giving an oversampling ratio of 8.44. The sample is a 7-μm tall "waving stick girl", pictured in Figure 7c), fabricated in a 100 nm thick silicon nitride window that is almost completely opaque at the CDL laser wavelength.

The coherent diffraction pattern was recorded after ~5.5 min exposure. Phase retrieval and the reconstruction were carried out by the guided hybrid-input-output (GHIO) algorithm [39, 44, 46] and a novel field curvature correction of the diffraction pattern. To achieve the best spatial resolution the detector was placed as close to the sample as possible increasing the NA of the system. At high NA $\sin(\alpha) \approx \alpha$ is no longer valid and the diffraction intensity on the planar CCD is significantly distorted. To avoid the distortion, the diffraction pattern, shown in Figure 7a) was projected from a plane onto a spherical surface – Ewald sphere. Figure 7b) shows the curvature-corrected diffraction pattern. Figure 7d)

Downloaded From: https://www.spiedigitallibrary.org/conference-proceedings-of-spie on 02 Aug 2019
Terms of Use: https://www.spiedigitallibrary.org/terms-of-use

show the magnitude of the reconstructed image from the curvature-corrected diffraction pattern, which is in excellent agreement with the SEM image of the object, shown in Figure 7c). A standard knife-edge resolution test was applied indicating a resolution of 71 nm, shown in Figure 7e). This resolution is approximately 1.5λ. The resolution is limited by the size of the CCD detector, because the diffraction pattern was clipped by the CCD edges. Moreover, the technique, despite its advantages, is affected by a complicated and time consuming GHIO phase retrieval algorithm comparing, for example, to the holographic Fresnel propagator reconstruction code.

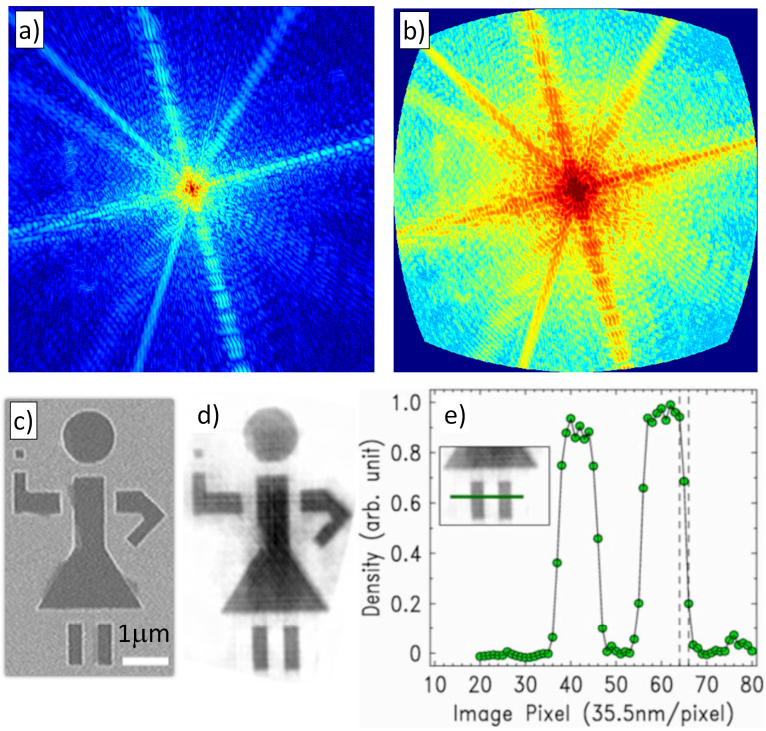


Figure 7. Diffraction pattern recorded on the CCD camera after stitching 3 diffraction patterns obtained using variable diameter beam blocks a), curvature corrected diffraction pattern b), SEM image of the object used in the experiment c), the magnitude of the reconstructed image from the curvature-corrected diffraction pattern d) and the knife edge resolution estimation e).

Similar lens-less diffraction imaging experiment was carried out using HHG source at 29 nm wavelength, also presented in [44], yielding a worse resolution of 92 nm, ~3.2λ, mainly due to lower temporal coherence (higher spectral bandwidth) of the HHG source compared with the EUV laser. It also requires much longer exposure as a result of much lower photon flux achievable with HHG source.

The diffractive imaging technique, coupled with compact and coherent short wavelength light sources, might soon enable tabletop EUV/SXR diffraction microscopy of materials and biological specimen with sub-10 nm resolution.

6. INCOHERENT EUV MICROSCOPY WITH ZONE PLATE OPTICS

Decreasing the illumination wavelength is one of the way to improve the spatial resolution in photon-based systems, thus the widespread applications of microscopy at EUV/SXR wavelengths require brighter and more compact short wavelength sources that will open the possibility to develop more compact and more widely accessible EUV/SXR microscopes.

Many imaging experiments were carried out so far, using coherent and incoherent EUV/SXR sources. A 700nm half-pitch resolution images with the use of EUV recombination laser at λ=18.2nm has been reported in the early imaging work [47]. Much better spatial resolution equal to 75nm was reported utilizing SXR laser at λ=4.48 nm, however, to pump this SXR laser a very large fusion-class NOVA laser was used, thus, image acquisition was limited by the repetition rate of a pumping laser to several shots per day [48]. Recently different approaches have emerged due to the

Downloaded From: https://www.spiedigitallibrary.org/conference-proceedings-of-spie on 02 Aug 2019
Terms of Use: https://www.spiedigitallibrary.org/terms-of-use

development of smaller-scale short-wavelength sources such as HHG [49], EUV lasers [50] and incoherent laser-plasma based sources [51] that have been successfully used for sub-micrometer resolution imaging. Using radiation from the CDL EUV images were obtained with a spatial resolution of 120-150nm [52]. 13.2nm wavelength radiation from Ni-like cadmium EUV laser allowed for a sub-38nm resolution nano-imaging [53], using pulses of 1J energy and ~8ps time duration for pumping the EUV laser. A quasi-monochromatic emission from an incoherent SXR source, at much shorter wavelength λ=2.88nm in the "water window" range, based on liquid nitrogen, allowed to demonstrate SXR microscopy with sub-50nm spatial resolution (~17λ) [54]. Till now to our knowledge, the best spatial resolution for photon-based zone plate microscopes, obtained so far is 12 nm, utilizing λ=1.7nm SXR radiation from a synchrotron source [55].

In this section an actinic tabletop EUV transmission microscope, using diffractive optic, will be presented. The microscope is presented in more detail in [56]. It uses a quasi-monochromatic, compact, high repetition rate, laser-plasma EUV source based on a gas puff target, discussed in Section 2. EUV radiation from the source is collected, focused and spectrally filtered by an ellipsoidal, off-axis, 80 mm in diameter mirror condenser with Mo/Si multilayers optimized for 13.5+/-0.5 nm (FWHM) wavelength range and 45 degrees incidence angle. The theoretical reflectivity of the mirror is ~34% for an unpolarized light at 13.8nm. The mirror was designed to image the plasma with a unity lateral magnification. The EUV radiation illuminates the object, positioned 254 mm downstream to the condenser. A 141 nm thick Zr filter (Luxel), positioned ~4-5 mm upstream to the object, is used to eliminate the wavelengths above 18 nm. The number of photons in the condenser focus is equal to $(8.8+/-0.5)x10^{10}$, as was reported in [8]. The source EUV spectrum, measured with the flat-field reflection grating spectrometer equipped with a 1200-line/mm variable groove spacing grating from Hitachi, has two main spectral peaks: $2p^63p-2p^65d$ at 13.793 nm and $2p^63s-2p^65p$ at 13.844 nm transitions in Ar VIII. Relative inverse bandwidth of the filtered spectrum is $\lambda/\Delta\lambda\sim140$ at λ=13.84 nm, but due to the relatively wide spectral response of our spectrometer (0.24 Å) this value might be underestimated.

The Fresnel zone plate (ZP) was used as an objective to image an object onto a EUV sensitive CCD camera iKon-M (Andor) with 1024x1024 pixels, 13x13 μm^2 pixel size. The ZP (from Zone Plates Ltd.) has a diameter of 200 μm and the outer zone width Δr=50 nm that yields to f=724.6 μm 1st order focal length at λ=13.8 nm wavelength and the numerical aperture NA=0.137. The microscope magnification is 468.3x and the image pixel size is 27.7 nm. The NA of the ZP matches the geometrical numerical apertures of the condenser in horizontal and vertical directions equal to 0.11 and 0.15, respectively, thus providing incoherent illumination. For precise object pre-focusing a piezoelectric, 25 μm travel, single axis flexure stage, NF15A (Thorlabs) is used, having a theoretical resolution of ~10 nm. Additional beam block, 12mm in diameter, was used to avoid stray light through the ZP, providing conical illumination. A single EUV image requires 200 EUV pulses, at the source repetition rate of 2 Hz. The object is a copper G2000HS Fine Square Mesh (SPI Supplies), used commonly in TEM calibration. Typical SEM image of the mesh is shown in Figure 8a). EUV microscope image of the mesh, with 12.5 μm period and 5 μm bar, is shown in Figure 8b).

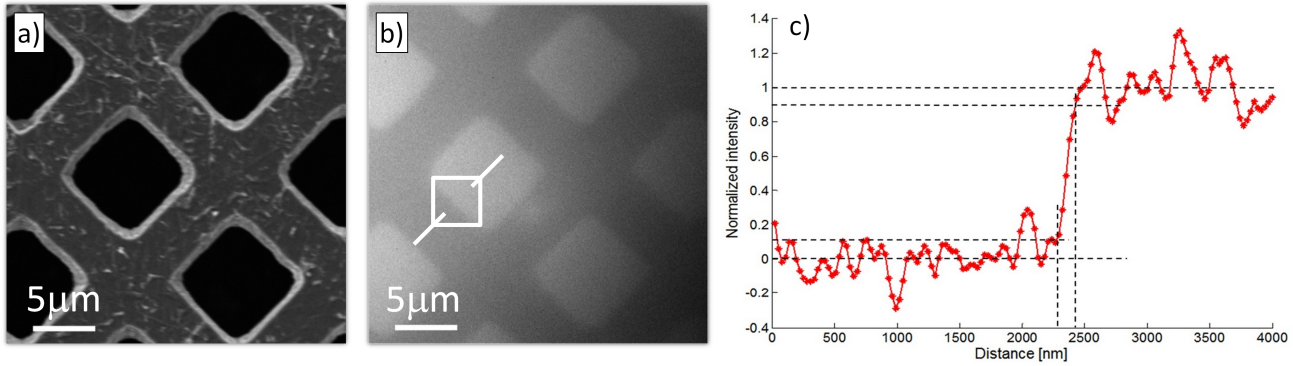


Figure 8. SEM image of the copper mesh with 12.5 μm period and 5 μm width bar a), EUV microscope image of the mesh, indicating region of interest for subsequent resolution evaluation b) and knife-edge resolution profile for the EUV image where he estimated 10 to 90% intensity transition across the sharp edge is equal to 138.5 nm (5 pixels) is shown in c).

Resolution of the microscope is assessed by the knife-edge test. The lineout across EUV image, indicated by two lines in Figure 8b), is depicted in Figure 8c) and is obtained by averaging 10 adjacent lines in the EUV image to improve the signal to noise ratio. The KE measurements yielded 10-90% resolution of 138.8+/-8.0 nm based on 10 measurements. This corresponds to a half-pitch spatial resolution of the microscope equal to 69.4+/-4.0 nm.

Downloaded From: https://www.spiedigitallibrary.org/conference-proceedings-of-spie on 02 Aug 2019
Terms of Use: https://www.spiedigitallibrary.org/terms-of-use

The experimental setup that was used in this EUV microscopy experiment is extremely compact. The setup consists of three small vacuum chambers. The microscope is located inside the vacuum chamber, 24 cm in diameter and 35 cm in length. The entire system fits on top of a single 2x0.6 m^2 optical table.

7. CONCLUSIONS

Different imaging techniques were presented in this paper that open a possibility to image a nanometer size objects at EUV wavelengths, with the spatial resolution approaching the wavelength of light used. Three different experiments in 2-D holographic imaging were presented. They show that the increase in the NA is a way to improve the spatial resolution yielding 380nm, 164nm and finally 45.8nm for the highest NA. Moreover 3-D information was extracted from a single, high NA, hologram with a spatial resolution of ~160nm and 2.1μm depth of focus.

Two new and simple imaging approaches, reconstruction of the computer generated holograms and generalized Talbot imaging at EUV wavelengths, having <90nm spatial resolution, are also discussed. Similarly to holography these methods do not require sophisticated optics, just a coherent illumination source and the hologram or self-imaging Talbot mask. This is particularly convenient in the EUV spectral region where the optics is expensive and difficult to fabricate. They are both self-correcting, immune to small imperfections in some unit cells in the Talbot mask or damage to a portion of a hologram and are scalable to shorter wavelengths, limited by the wavelength of the source, its coherence and the ability to fabricate either hologram or the Talbot mask with a certain accuracy and resolution.

Another, very interesting and important imaging technique, presented in this paper, is a diffractive lens-less imaging, achieving resolution approaching 70nm. This scalable to shorter wavelengths technique should be suitable to achieve sub-10 nm resolution imaging of a wide range of specimens in biology, materials science, nanoscience and nanotechnology. Higher repetition-rate lasers, faster de-convolution algorithms using parallel codes and improved phase retrieval techniques may help reaching this goal.

All the techniques, presented above, require coherent light, which is more difficult to achieve. However, high resolution EUV imaging can also be done using incoherent plasma sources. A tabletop, EUV transmission microscope, based on a Fresnel diffractive optic and a compact, laser-plasma EUV source, was presented. The microscope, under the incoherent illumination, allows to capture images at 13.8 nm wavelength with the spatial resolution of 69 nm in a short exposure time. These results should be useful for the realization of high resolution, compact, table-top imaging systems for studying a variety of specimen in biology, material science and nanotechnology.

All presented methods are table-top, where the whole set up fits on top of an optical table, bringing to the laboratory environment similar, high resolution imaging capabilities as available in large synchrotron facilities. The continuing development of highly coherent table-top EUV lasers in the vicinity of 10 nm [57] and increase in the available flux will enable single shot recording, permitting full field and time resolved high resolution imaging utilizing some of the techniques presented herein. Moreover photon based imaging systems allow spectroscopic contrast, an important characteristic in imaging with shorter wavelength radiation. It also opens the possibility to study specimens in different environments, for example in the presence of external magnetic or electric fields.

8. ACKNOWLEDGEMENTS

The research was partially supported by Foundation for Polish Science HOMING 2009 Programme (grant number HOM2009/14B), EC's 7. Framework Program LASERLAB-EUROPE - grant agreement n° 228334, COST Action MP0601, European Economic Area (EEA) Grants, NER program, NSF Award DMI-0508484, NSF ERC for Extreme Ultraviolet Science and Technology, Award Number EEC-0310717, EUREKA project Σ! 3892 ModPolEUV, Ministry of Science and Higher Education of Poland (decision Nr 120/EUR/2007/02). We would like to thank to Dr. R. Jarocki, Dr. J. Kostecki, Dr. R. Rakowski, and Dr. M. Szczurek, for their contribution in the development of the gas puff target EUV source. P.W.W wishes to thank the organizers of the 17th SLOVAK-CZECH-POLISH OPTICAL CONFERENCE, Wave and Quantum Aspects of Contemporary Optics, for the invitation and the opportunity to present the work described in this paper.

Downloaded From: https://www.spiedigitallibrary.org/conference-proceedings-of-spie on 02 Aug 2019
Terms of Use: https://www.spiedigitallibrary.org/terms-of-use

REFERENCES

[1] J. J. Rocca, V. Shlyaptsev, F. G. Tomasel, O. D. Cortázar, D. Hartshorn, and J. L. A. Chilla, "Demonstration of a Discharge Pumped Table-Top Soft-X-Ray Laser", Physical Review Letters 73 (16), 2192 (1994).

[2] B. R. Benware, C. D. Macchietto, C. H. Moreno, J. J. Rocca, "Demonstration of a High Average Power Tabletop Soft X-Ray Laser", Physical Review Letters 81 (26), 5804 (1998)

[3] C. D. Macchietto, B. R. Benware, and J. J. Rocca, "Generation of millijoule-level soft-x-ray laser pulses at a 4-Hz repetition rate in a highly saturated tabletop capillary discharge amplifier," Opt. Lett. 24, 1115-1117 (1999)

[4] Y. Liu, M. Seminario, F. G. Tomasel, C. Chang, J. J. Rocca and D. Attwood,"Achievement of essentially full spatial coherence in a high-average-power soft-x-ray laser". Phys. Rev. A, 6303, 033802, (2001).

[5] C. A. Brewer, F. Brizuela, P. Wachulak, D. H. Martz, W. Chao, E.H. Anderson, D.T. Attwood, A. V. Vinogradov, I. A. Artyukov, A.G. Ponomareko, V.V. Kondratenko, M.C. Marconi, J.J. Rocca, C.S. Menoni, "Single-shot extreme ultraviolet laser imaging of nanostructures with wavelength resolution", Optics Letters, 33, 518, (2008), Virtual Journal for Biomedical Optics, 3, 4, (2008) and in Virtual Journal of Nanoscale Science & Technology, 17, 15, (2008)

[6] H. Fiedorowicz, A. Bartnik, R. Jarocki, J. Kostecki, J. Krzywinski, J. Mikołajczyk, R. Rakowski, A. Szczurek, M. Szczurek, "Compact laser plasma EUV source based on a gas puff target for metrology applications", J. Alloys Compd. 401, 99–103 (2005).

[7] R.Rakowski, A. Bartnik, H. Fiedorowicz, R. Jarocki, J. Kostecki, J. Krzywiński, J. Mikołajczyk, L. Pina, L. Ryć, M. Szczurek, H. Ticha, P. Wachulak, "Metrology of Mo/Si multilayer mirrors at 13.5 nm with the use of a laser-produced plasma extreme ultraviolet (EUV) source based on a gas puff target", Optica Applicata, 36, 4, (2006)

[8] P. W. Wachulak, A. Bartnik, H. Fiedorowicz, T. Feigl, R. Jarocki, J. Kostecki, R. Rakowski, P. Rudawski, M. Sawicka, M. Szczurek, A. Szczurek, Z. Zawadzki, "A compact, quasi-monochromatic laser-plasma EUV source based on a double stream gas puff target at 13.8nm wavelength", Applied Physics B 100, 3, 461-469, (2010).

[9] D. Gabor, "A new microscopic principle". Nature, 161, 777, (1948)

[10] A. V. Baez. "A study in diffraction microscopy with special reference to X-rays". Journal of the Optical Society of America, 42, 756, (1952)

[11] E. N. Leith and J. Upatnieks. "Reconstructed Wavefronts And Communication Theory", Journal of the Optical Society of America, 52, 1123, (1962)

[12] P. W. Wachulak, M. C. Marconi, R. A. Bartels, C. S. Menoni, J. J. Rocca, "Holographic imaging with a nanometer resolution using compact table-top EUV laser", Opto-electronics review 18, 1, 28-38 (2010)

[13] J. W. Giles. "Image reconstruction from a Fraunhofer X-ray hologram with visible light". Journal of the Optical Society of America, 59, 1179, (1969)

[14] S. Aoki and S. Kikuta. "X ray holographic microscopy". Jpn. J. Appl. Phys., 13, 1385, (1974)

[15] C. Jacobsen, et al., "X-Ray Holographic Microscopy Using Photoresists", Journal Of The Optical Society Of America A-Optics Image Science And Vision, 1990. 7(10): p. 1847-1861.

[16] S. Lindaas, H. Howells, C. Jacobsen, and A. Kalinovsky, "X-ray holographic microscopy by means of photoresist recording and atomic-force microscope readout". Journal of the Optical Society of America a-Optics Image Science and Vision. 13(9): p. 1788-1800.(1996).

[17] R.A. Bartels, A. Paul, H. Green, H.C. Kapteyn, M.M. Murnane, S. Backus, I.P. Christov, Y.W. Liu, D. Attwood, and C. Jacobsen, "Generation of spatially coherent light at extreme ultraviolet wavelengths", Science. 297(5580): p. 376-378,(2002).

[18] A.S. Morlens, J. Gautier, G. Rey, P. Zeitoun, J.P. Caumes, M. Kos-Rosset, H. Merdji, S. Kazamias, K. Casson, and M. Fajardo, "Submicrometer digital in-line holographic microscopy at 32 nm with high-order harmonics". Optics Letters. 31(21): p. 3095-3097, (2006).

[19] R.I. Tobey, M.E. Siemens, O. Cohen, M.M. Murnane, H.C. Kapteyn, and K.A. Nelson, "Ultrafast extreme ultraviolet holography: dynamic monitoring of surface deformation". Optics Letters. 32(3): p. 286-288.(2007).

[20] P. Wachulak, R. Bartels, M.C. Marconi, C.S. Menoni, J.J. Rocca,Y. Lu, B. Parkinson, "Sub 400 nm spatial resolution extreme ultraviolet holography with a table top laser". Optics Express. 14(21): p. 9636-9642.(2006).

[21] P. Wachulak, M.C. Marconi, R. Bartels, C.S. Menoni, J.J. Rocca, "Volume extreme ultraviolet holographic imaging with numerical optical sectioning". Optics Express. 15: p. 10622-10628.(2007).

Downloaded From: https://www.spiedigitallibrary.org/conference-proceedings-of-spie on 02 Aug 2019
Terms of Use: https://www.spiedigitallibrary.org/terms-of-use

[22] P. W. Wachulak, M.C. Marconi, R. A. Bartels, C. S. Menoni, J.J. Rocca, “Soft x-ray laser holography with wavelength resolution“, J. Opt. Soc. Am. B, 25, 11, 1811 (2008)
[23] J. Goodman, W., “Introduction to Fourier Optics”, (McGraw Hill, 1996): p. Chap 4, p. 66.
[24] U. Schnars and W.P.O. Juptner, “Digital recording and reconstruction of holograms in hologram interferometry and shearography”, Applied Optics, 1994. 33(20): p. 4373-4377.
[25] U. Schnars and W.P.O. Juptner, “Digital recording and numerical reconstruction of holograms”, Measurement Science & Technology, 2002. 13(9): p. R85-R101.
[26] A. C. F. Hoole, M. E. Welland, A. N. Broers, “Negative PMMA as a high-resolution resist - the limits and possibilities”, Semicond. Sci. Technol. 12, 1166-1170 (1997)
[27] K. Yamazaki, T. Yamaguchi, H. Namatsu, “Three-Dimensional Nanofabrication with 10-nm Resolution”, Jpn. J. Appl. Phys. 43, L1111-L1113 (2004)
[28] J. M. Heck, D. T. Attwood, W. Meyer-Ilse, E. H. Anderson, “Resolution determination in X-ray microscopy: an analysis of the effects of partial coherence and illumination spectrum”, Journal of X-Ray Science and Technology 8, 95 (1998)
[29] P.W. Wachulak, Brewer, C.A., Brizuela, F., Chao, W., Anderson, E.H., Bartels, R.A., Menoni, C.S., Rocca, J.J., Marconi, M.C., “Simultaneous determination of feature size and resolution in soft x-ray microscopy images”. Journal of the Optical Society of America B. 25 B20-B26 (2008).
[30] CXRO, "http://www-cxro.lbl.gov/".
[31] From Polysciences Inc.
[32] D. Attwood, Soft X-ray and extreme ultraviolet radiation, (Cambridge University Press. 1999)
[33] M.R. Howells and C. Jacobsen, "Possibilities for Projection X-ray Lithography Using Holographic Optical Elements". Applied Optics. 30 1580-1582 (1991).
[34] Y.-C. Cheng, A. Isoyan, J. Wallace, M. Khan, and F. Cerrina, "Extreme ultraviolet holographic lithography: Initial results", Applied Physics Letters. 90 023116 (2007).
[35] A. Isoyan, F. Jian, Y. Cheng, P. Wachulak, L. Urbanski, J. Rocca, C. Menoni, M. C. Marconi, and F. Cerrina, "Coherent Imaging Nano-Patterning with Extreme Ultraviolet Laser Illumination," in Conference on Lasers and Electro-Optics/International Quantum Electronics Conference, OSA Technical Digest (CD) (Optical Society of America, 2009), paper JFA7, http://www.opticsinfobase.org/abstract.cfm?URI=CLEO-2009-JFA7
[36] A. Isoyan, F. Jiang, Y. C. Cheng, F. Cerrina, P. Wachulak, L. Urbanski, J. Rocca, C. Menoni, and M. Marconi, “Talbot lithography: Self-imaging of complex structures”, Journal of Vacuum Science & Technology B, 27, 6 , 2931-2937 (2009)
[37] J. W. Miao, H. N. Chapman, J. Kirz, D. Sayre, K. O. Hodgson, “Taking X-ray diffraction to the limit: Macromolecular structures from femtosecond X-ray pulses and diffraction microscopy of cells with synchrotron radiation”, Annual Review of Biophysics and Biomolecular Structure 33, 157 (2004).
[38] J. W. Miao, P. Charalambous, J. Kirz et al., "Extending the methodology of X-ray crystallography to allow imaging of micrometre-sized non-crystalline specimens," Nature 400 (6742), 342-344 (1999).
[39] J. Miao, C. Chen, C. Song, Y. Nishino, Y. Kohmura, T. Ishikawa, D. Ramunno-Johnson, T. Lee, and S. H. Risbud, “Three-Dimensional GaN-Ga_2O_3 Core Shell Structure Revealed by X-Ray Diffraction Microscopy”, Phys. Rev. Lett. 97, 215503 (2006).
[40] D. Shapiro, P. Thibault, T. Beetz, V. Elser, M. Howells, C. Jacobsen, J. Kirz, E. Lima, H. Miao, A. M. Neiman, and D. Sayre, “Biological imaging by soft x-ray diffraction microscopy”, Proceedings of the National Academy of Sciences of the United States of America 102 (43), 15343 (2005).
[41] S. Elsebitt, W. F. Schlotter, M. Lorgen, O. Hellwig, W. Eberhardt, J. Stohr, “Lensless imaging of magnetic nanostructures by x-ray spectro holography”. Nature, 432, 885, (2004).
[42] J. W. Miao, K. O. Hodgson, and D. Sayre,” An approach to three-dimensional structures of biomolecules by using single-molecule diffraction images”, Proceedings of the National Academy of Sciences of the United States of America 98 (12), 6641 (2001).
[43] H. N. Chapman, A. Barty, M. J. Bogan et al., “Femtosecond diffractive imaging with a soft-X-ray free-electron laser”, Nature Physics 2 (12), 839 (2006).
[44] R.L. Sandberg, C. Song, P.W. Wachulak, D.A. Raymondson, A. Paul, B. Amirbekian, E. Lee, A. Sakdinawat, C.L. Vorakiat, M.C. Marconi, C.S. Menoni, M.M. Murnane, J.J. Rocca, H.C. Kapteyn, J. Miao, “High numerical aperture tabletop soft x-ray diffraction microscopy with 70 nm resolution”, Proceedings of the National Academy of Science, 105, (1), 24-27, (2008), highlighted in Nature Photonics 2, 64 (2008)

Downloaded From: https://www.spiedigitallibrary.org/conference-proceedings-of-spie on 02 Aug 2019
Terms of Use: https://www.spiedigitallibrary.org/terms-of-use

[45] J. Miao, D. Sayre, and H. N. Chapman, "Phase retrieval from the magnitude of the Fourier transforms of nonperiodic objects", Journal of the Optical Society of America a-Optics Image Science and Vision 15 (6), 1662 (1998).
[46] J. Miao, T. Ishikawa, E. H. Anderson and K. O. Hodgson, "Phase Retrieval of Diffraction Patterns from Non-Crystalline Samples", Phys. Rev. B 67, 174104 (2003).
[47] D. S. DiCicco, D. Kim, R. Rosser, and S. Suckewer, "First stage in the development of a soft-x-ray reflection imaging microscope in the Schwarzschild configuration using a soft-x-ray laser at 18.2nm", Optics Letters 17, 2, 157 (1992).
[48] L. B. Da Silva, J. E. Trebes, S. Mrowka, T. W. Barbee, Jr., J. Brase, J. A. Koch, R. A. London, B. J. MacGowan, D. L. Matthews, D. Minyard, G. Stone, T. Yorkey, E. Anderson, D. T. Attwood, and D. Kern, "Demonstration of x-ray microscopy with an x-ray laser operating near the carbon K edge", Optics Letters 17, 754 (1992).
[49] M. Wieland, C. Spielmann, U. Kleineberg, T. Westerwalbesloh, U. Heinzmann, and T. Wilhein, "Toward time-resolved soft X-ray microscopy using pulsed fs-high-harmonic radiation", Ultramicroscopy 102, 93 (2005).
[50] M.Kishimoto, M.Tanaka, R.Tai, K.Sukegawa, M. Kado, N.Hasegawa, H.Tang, T.Kawachi, P.Lu, K. Nagashima, H.Daido, Y.Kato, K.Nagai, and H. Takenaka, "Development of soft X-ray microscopy System using X-ray laser in JAERI Kansai", Journal de Physique IV 104, 141 (2003)
[51] I.A. Artioukov, A.V. Vinogradov, V.E. Asadchikov, Y.S. Kasyanov, R.V. Serov, A.I. Fedorenko, V.V. Kondratenko and S.A. Yulin, "Schwarzschild soft-x-ray microscope for imaging of nonradiating objects", Optics Letters 20, 2451 (1995)
[52] G. Vaschenko, F. Brizuela, C. Brewer, M. Grisham, H. Mancini, C.S. Menoni, M.C. Marconi, J.J. Rocca, W. Chao, J.A. Liddle, E.H. Anderson, D.T. Attwood, A.V. Vinogradov, I.A. Artioukov, Y.P. Pershyn, V.V. Kondratenko, "Nanoimaging with a compact extreme-ultraviolet laser", Optics Letters 30, 16, 2095 (2005)
[53] G.Vaschenko, C.Brewer, F.Brizuela, Y.Wang, M.A.Larotonda, B.M.Luther, M.C.Marconi, J.J.Rocca, and C.S.Menoni, "Sub-38nm resolution table top microscopy with 13nm wavelength laser light", Optics Letters 31, 9, 1214 (2006)
[54] K. W. Kim, Y. Kwon, K.Y. Nam, J.H. Lim, K.G. Kim, K.S. Chon, B.H. Kim, D.E. Kim, J.G. Kim, B.N. Ahn, H.J. Shin, S. Rah, K.H. Kim, J.S. Chae, D.G. Gweon, D.W. Kang, S.H. Kang, J.Y. Min, K.S. Choi, S.E. Yoon, E.A. Kim, Y. Namba and K.H. Yoon, "Compact soft x-ray transmission microscopy with sub-50nm spatial resolution", Physics in Medicine and Biology 51, N99-N107 (2006)
[55] W. Chao, J. Kim, S. Rekawa, P. Fischer and E. H. Anderson, "Demonstration of 12 nm Resolution Fresnel Zone Plate Lens based Soft X-ray Microscopy", Optics Express 17, 20, 17699 (2009)
[56] P. W. Wachulak, A. Bartnik and H. Fiedorowicz, "Sub-70nm resolution table top microscopy at 13.8nm using a compact laser–plasma EUV source", Optics Letters 35, 14, 2337-2339 (2010)
[57] Y. Wang, E. Granados, M.A. Larotonda, M. Berrill, B.M. Luther, D. Patel, C.S. Menoni, and J.J. Rocca, "High-brightness injection-seeded soft-x-ray-laser amplifier using a solid target". Physical Review Letters. 97 (2006).

Downloaded From: https://www.spiedigitallibrary.org/conference-proceedings-of-spie on 02 Aug 2019
Terms of Use: https://www.spiedigitallibrary.org/terms-of-use